

Monotop phenomenology at the Large Hadron Collider

Jean-Laurent Agram,¹ Jeremy Andrea,² Michael Buttignol,¹ Eric Conte,¹ and Benjamin Fuks^{2,3}

¹*Groupe de Recherche de Physique des Hautes Energies (GRPHE), Université de Haute-Alsace,
IUT Colmar, 34 rue du Grillenbreit BP 50568, 68008 Colmar Cedex, France*

²*Institut Pluridisciplinaire Hubert Curien/Département Recherches Subatomiques,
Université de Strasbourg/CNRS-IN2P3, 23 Rue du Loess, F-67037 Strasbourg, France*

³*Theory Division, Physics Department, CERN, CH-1211 Geneva 23, Switzerland*

(Dated: May 16, 2018)

We investigate new physics scenarios where systems comprised of a single top quark accompanied by missing transverse energy, dubbed monotops, can be produced at the LHC. Following a simplified model approach, we describe all possible monotop production modes via an effective theory and estimate the sensitivity of the LHC, assuming 20 fb^{-1} of collisions at a center-of-mass energy of 8 TeV, to the observation of a monotop state. Considering both leptonic and hadronic top quark decays, we show that large fractions of the parameter space are reachable and that new physics particles with masses ranging up to 1.5 TeV can leave hints within the 2012 LHC dataset, assuming moderate new physics coupling strengths.

PACS numbers: 12.38.Bx,12.60.-i,14.65.Ha

I. INTRODUCTION

After almost half a century, the Standard Model of particle physics has been proved to largely describe all experimental high-energy physics data. Despite its success, it however leaves many questions unanswered so that it is believed to be the low-energy limit of a more fundamental theory that is still to be discovered. Whilst there is currently no hint for any physics beyond the Standard Model, new phenomena are still actively searched for experimentally whereas on the theory side, model building activities are ongoing quite intensely for the last decades. In particular, the sector of the top quark whose mass is close to the electroweak symmetry breaking scale is expected to be one of the key candle for the possible discovery of new physics of any kind.

In the framework of the Standard Model, top quarks are mainly produced, at the Large Hadron Collider (LHC), either in pairs or singly via weak subprocesses. In this work, we focus on an additional production channel where the top quark is produced as a component of a monotop state, *i.e.*, in association with missing transverse energy. While such a system cannot be produced at current collider experiments in the context of the Standard Model due to loop-suppression and the Glashow-Iliopoulos-Maiani mechanism, large classes of new physics theories predict its possible observation. Among those, a first type of scenarios features a monotop signature arising from the decay of a heavy resonance. As examples, one finds supersymmetric models with R -parity violation in which a singly-produced top squark decays into a top quark and a long-lived neutralino giving rise to missing transverse energy [1–3], models with an extended gauge symmetry featuring leptoquarks that can decay into a particle pair constituted of a top quark and a neutrino [4] or hylogenesis scenarios for dark matter where the top quark is produced together with several dark matter candidates carrying missing momentum [5]. A second category of beyond the Standard Model theories leading to monotop production at the LHC with a possibly large rate exhibits flavor-changing neutral interactions of quarks, and in particular of the top quark, with fields belonging to a hidden sector. If produced in a collider experiment, these fields are hence manifest through a significant presence of missing transverse energy. In this theoretical framework, the specific example of a Z' field dominantly decaying invisibly and coupling to quarks in a flavor-violating fashion has recently received a particular attention as motivated by possible solutions to the dark matter problem of the Standard Model [6, 7].

While all these models are inspired by the so-called top-down approach for new physics investigations, an alternative choice focuses on the systematization of the analysis of a given beyond the Standard Model effect or signature. It relies on a bottom-up avenue where the Standard Model is extended minimally through the construction of an effective theory sufficient to reproduce the effect under consideration. More general monotop investigations have followed this path, concentrating either on the resonant production mode [8], on the derived effective four-fermion interactions that arise when the resonances are heavy [9, 10], on monotop production through flavor-changing neutral interactions [11] or on all cases simultaneously described via the most possibly general and renormalizable Lagrangian description [12]. In particular, the parameters of a part of the non-resonant production mechanisms included in this last Lagrangian, that is also motivated by a possible explanation for several new physics signals reported by dark matter direct detection experiments [13–16], have already been constrained by a recent analysis of all Tevatron data by the CDF collaboration [17]. It has been found that light vector states leading to missing transverse energy in the detector and interacting in a flavor-violating fashion with the quarks are restricted to be heavier than about 100 GeV at the 95% confidence level.

In this work, we revisit and update a pioneering analysis of the LHC sensitivity to monotops based on the most general and renormalizable dedicated effective field theory. In this context, the Standard Model is supplemented by a series of dimension-four operators and new states, the corresponding Lagrangian encompassing all possible monotop production modes [12]. However, this analysis has been first restricted to an estimate of the LHC reach to monotops decaying only into a purely hadronic state. Additionally, it has been based on parton-level Monte Carlo simulations of collisions that have been produced during the 2011 run of the LHC collider, at a center-of-mass energy of 7 TeV. A detailed investigation of the monotop phenomenology at the LHC, employing the above-mentioned framework, considering both the hadronic and leptonic decay modes and focusing on the 2012 LHC run, is therefore still missing.

This paper has the aim to fill this gap and provides, by means of state-of-the-art Monte Carlo event generation, a first estimate of the LHC sensitivity to monotops by making use of the 2012 dataset. We base our analysis on a simulation of 20 fb^{-1} of proton-proton collisions at a center-of-mass energy of 8 TeV and achieve an accurate background description by using multiparton matrix-element merging techniques, precise total cross section predictions for the Standard Model background subprocesses as well as an advanced modeling of the effects yielded by a CMS-like detector. Within this setup, we design several search strategies that we think worthwhile to be tested in the context of the real data by both the ATLAS and CMS experiments. All of them rely on the amount of missing transverse energy accompanying the top quark which is expected to be important. In our simplified model approach, this missing transverse energy is assumed to be due to a neutral weakly interacting new physics state either of spin zero, one-half or one, and that is also possibly a candidate for explaining the presence of dark matter in the Universe. This new particle is then either long-lived or stable so that it is prevented to leave any visible track in the detector. In addition,

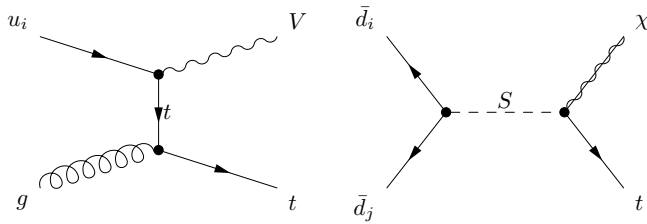


FIG. 1. Representative Feynman diagrams leading to a monotop signature, either through a flavor-changing neutral interaction of an up-type quark with a vector state V (left) or via the resonant exchange of a colored scalar field S (right). The final state particles V and χ are invisible.

the study of the hadronic monotop signature employs the strength of the possible top quark reconstruction to reject most of the background [6, 8, 12], whereas the extraction of a leptonic monotop signal is based in on the calculation of the transverse mass of the two-body system comprised of the lepton issued from the top quark decay and the missing transverse momentum [7].

This work is organized as follows. In Section II, we review the effective field theory that has been constructed to describe all possible monotop production mechanisms and that we have employed in our analysis. In addition, we carefully investigate the associated total cross sections as a function of the different model parameters in order to get a first idea about the mass range expected to be reachable at the LHC running at a center-of-mass energy of 8 TeV. We detail in Section III the phenomenological analyses that we have designed in the aim of unveiling new physics arising through a monotop signature at the LHC. We first describe our Monte Carlo simulation setup in Section III.1 and then proceed with the analysis of the hadronic and leptonic monotop final states in Section III.2 and Section III.3, respectively. Our conclusions are given in Section IV.

II. THEORETICAL FRAMEWORK

As presented in earlier studies, there are two different types of tree-level processes yielding the production of a monotop state [12]. This classification depends on the nature of the particle giving rise to missing transverse energy. More into details, either the top quark is produced through a flavor-changing neutral interaction with a lighter quark and a new invisible bosonic state¹, as illustrated by the representative Feynman diagram of the left panel of Figure 1, or in association with an invisible fermionic state as shown on the representative Feynman diagram of the right panel of Figure 1. Starting from the Standard Model, we describe all these monotop production mechanisms by constructing a simplified model whose Lagrangian is given, when omitting exotic monotop production mechanisms involving fields with a spin higher than one or higher-dimensional operators, by

$$\begin{aligned}
 \mathcal{L} = & \mathcal{L}_{\text{SM}} + \mathcal{L}_{\text{kin}} + \left[\phi \bar{u} \left[a_{FC}^0 + b_{FC}^0 \gamma_5 \right] u + V_\mu \bar{u} \gamma^\mu \left[a_{FC}^1 + b_{FC}^1 \gamma_5 \right] u \right. \\
 & + \varphi \bar{d}^c \left[a_{SR}^q + b_{SR}^q \gamma_5 \right] d + \varphi \bar{u} \left[a_{SR}^{1/2} + b_{SR}^{1/2} \gamma_5 \right] \chi \\
 & \left. + X_\mu \bar{d}^c \gamma^\mu \left[a_{VR}^q + b_{VR}^q \gamma_5 \right] d + X_\mu \bar{u} \gamma^\mu \left[a_{VR}^{1/2} + b_{VR}^{1/2} \gamma_5 \right] \chi + \text{h.c.} \right].
 \end{aligned} \tag{2.1}$$

In this approach, the Standard Model Lagrangian \mathcal{L}_{SM} is first supplemented by kinetic and gauge interaction terms for all new states included in the Lagrangian \mathcal{L}_{kin} . Next, we depict the flavor-changing associated production of a top quark and a scalar ϕ or vector V invisible state by the other terms of the first line of the equation above, all color and generation indices being understood for clarity. The strength of the interactions among these two states and a pair of up-type quarks is modeled via two 3×3 matrices in flavor space $a_{FC}^{\{0,1\}}$ and $b_{FC}^{\{0,1\}}$. The last two lines of the Lagrangian of Eq. (2.1) are related to the second considered class of processes leading to the production of a monotop system comprised in this case of a top quark and an invisible fermionic state χ . In this work, we restrict ourselves to a production mechanism involving the decay of a new colored, scalar φ or vector X , resonance lying in the fundamental representation of the QCD group $SU(3)_c$. In our notations, the couplings of these new colored fields

¹ We denote by invisible any state whose signature in a detector consists of missing transverse energy.

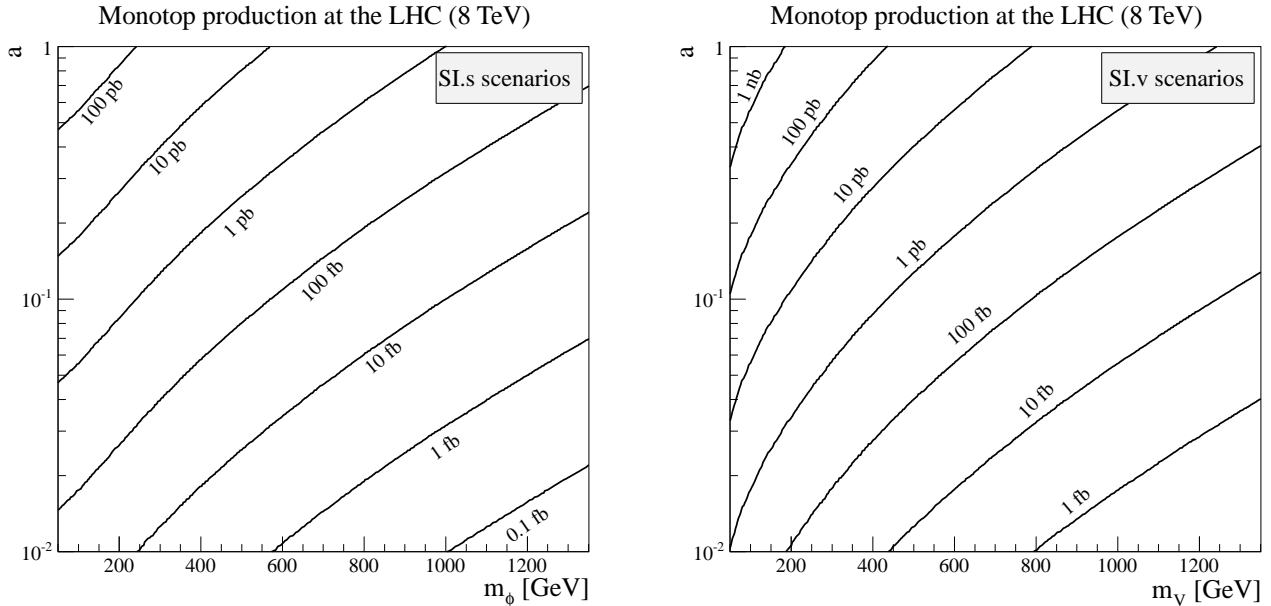


FIG. 2. Total cross sections for monotop production at the LHC, running at a center-of-mass energy of 8 TeV, for scenarios of type **SI.s** (left panel) and **SI.v** (right panel). The results are given as a function of the new physics coupling a and the invisible particle mass m_ϕ (scalar case) and m_V (vector case).

to down-type quarks are embedded into the 3×3 matrices $a_{\{S,V\}R}^q$ and $b_{\{S,V\}R}^q$ while those to the invisible fermion χ and one single up-type quarks are given by the three-component vectors $a_{\{S,V\}R}^{1/2}$ and $b_{\{S,V\}R}^{1/2}$ in flavor space.

Starting from the large series of monotop benchmark models included in the Lagrangian of Eq. (2.1), we consider a set of simplified scenarios in which all axial couplings vanish,

$$b = 0 . \quad (2.2)$$

Furthermore, we adopt a LHC point of view and only retain interactions possibly enhanced by parton densities in the proton. We hence fix

$$\begin{aligned} (a_{FC}^0)_{13} &= (a_{FC}^0)_{31} = (a_{FC}^1)_{13} = (a_{FC}^1)_{31} = a , \\ (a_{SR}^q)_{12} &= -(a_{SR}^q)_{21} = (a_{SR}^{1/2})_3 = (a_{VR}^q)_{11} = (a_{VR}^{1/2})_3 = a , \end{aligned} \quad (2.3)$$

the other elements of the coupling matrices being set to zero. Within the above settings, we define four series of scenarios. The first two are denoted by **SI.s** and **SI.v** and address monotop production via baryon-number conserving and flavor-changing neutral interactions in the case where a single scalar (**SI.s**) or vector (**SI.v**) field is added to the Standard Model. These new fields are assumed to be either stable or to decay invisibly, so that they yield missing transverse energy when produced in a collider experiment. The last two sets of scenarios, that we denote by **SII.s** and **SII.v**, focus on the production of a monotop state via the decay of a new scalar (**SII.s**) or vector (**SII.v**) colored resonance. We further assume, in our simplified setup, that the new resonances always decay with a branching ratio equal to unity into a monotop state. While this assumption is in general too optimistic when one accounts for the dijet decay mode [8], it however has the advantage to simplify the benchmark scenario design as it allows monotop production to be insensitive to the a_{SR}^q and a_{VR}^q parameters.

For each of these classes of scenarios, we estimate monotop production cross sections at the LHC, running at a center-of-mass energy of $\sqrt{S_h} = 8$ TeV, by means of the QCD factorization theorem. We convolute the partonic results $\hat{\sigma}$ as computed by MADGRAPH 5 [18] with the leading order set of the CTEQ6 fit [19] of the universal parton densities $f_{a,b}$ of partons a, b in the proton. Introducing the longitudinal momentum fractions of the two partons $x_{a,b} = \sqrt{\tau} e^{\pm y}$, the total cross sections σ are hence given by

$$\sigma = \sum_{a,b} \int_{\tilde{M}^2/S_h}^1 d\tau \int_{-1/2 \ln \tau}^{1/2 \ln \tau} dy f_a(x_a, \mu_F^2) f_b(x_b, \mu_F^2) \hat{\sigma}(x_a x_b S_h, \mu_R) . \quad (2.4)$$

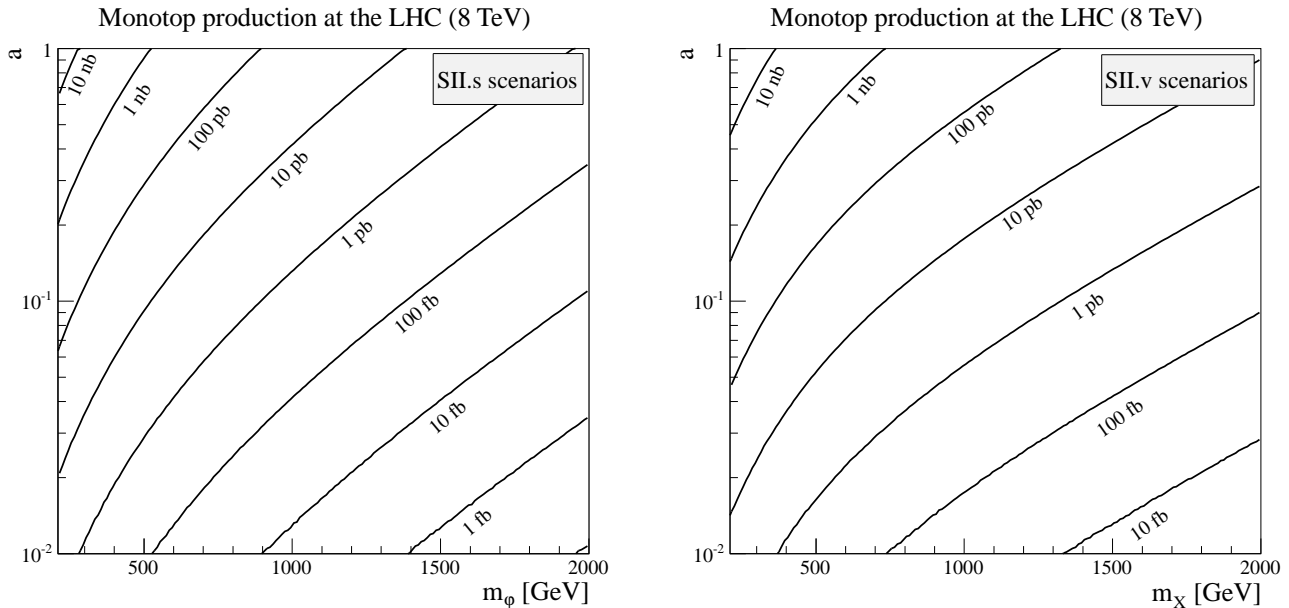


FIG. 3. Total cross sections for monotop production at the LHC, running at a center-of-mass energy of 8 TeV, for scenarios of type **SII.s** (left panel) and **SII.v** (right panel). The branching fraction of the resonant state into a monotop system is assumed to be unity and the results are given as a function of the new physics coupling a and of the resonance mass m_ϕ (scalar resonance) or m_X (vector resonance).

In our calculations, we fix both the renormalization and factorization scales μ_F and μ_R to the transverse mass of the monotop system whose production threshold is denoted by \tilde{M} and we sum the results related to the production of a top and an antitop quark in association with missing transverse energy.

In scenarios of class **SI.s** and **SI.v**, a top quark is produced in association with a bosonic particle through a flavor-changing interaction, this bosonic particle being invisible and giving rise to missing transverse energy. These two classes of scenarios are described by two parameters, the mass of the missing transverse energy particle m_ϕ (for **SI.s** scenarios) and m_V (for **SI.v** scenarios) and the strength a of the flavor-changing interactions of these particles with a pair of quarks constituted of one top quark and one up quark, as introduced in Eq. (2.3). In Figure 2, we present monotop production cross sections as a function of these two parameters for a scalar (left panel of the figure) and vector (right panel of the figure) invisible state. We find that cross sections reaching at least 1 pb can be easily obtained even for moderate coupling strengths of about $a \approx 0.1$. Conversely, such a coupling value implies that in the context of scenarios of type **SI.s** (**SI.v**), monotop systems containing an invisible particle of mass ranging up to about 300 GeV (500 GeV) could have been abundantly produced during the 2012 LHC run. Furthermore, scenarios featuring an invisible vector field lead to a larger total cross section at the LHC than in the scalar case, when considering a specific mass and coupling strength. This directly originates from the vectorial nature of the invisible field included in **SI.v** scenarios.

In scenarios of type **SII.s** and **SII.v**, we consider that the monotop state arises from the decay, with a branching fraction equal to unity, of a new colored scalar φ or vector X resonance. In this case, the missing transverse energy is induced by an undetected fermionic field that we denote by χ . These two classes of scenarios are described by three parameters, the coupling strength of the down-type quarks to the new resonance a , the resonance mass m_φ (for **SII.s** scenarios) and m_X (for **SII.v** scenarios) and the mass of the invisible particle m_χ . Monotop production cross sections are however independent of the invisible particle mass as they are equal to the production cross section of the φ or X field multiplied by the subsequent branching ratio into a $t\chi$ pair (being here set to one). The mass difference between the resonance and the missing transverse energy particle however alters the selection efficiency of any monotop search strategy as it is related to the phase space available for the resonance decay. The dependence of the monotop production cross section on the resonance mass and on the new physics coupling strength a is presented on Figure 3 for scenarios involving either a scalar resonance (left panel of the figure) or a vector resonance (right panel of the figure). Cross sections reaching the level of a few pb, allowing for a large production of monotop events at the LHC, are predicted for a moderate coupling strength of $a \approx 0.1$ and for resonance masses ranging up to about 1 TeV and 1.3 TeV in the scalar and vector cases, respectively. This difference finds again its source in the larger cross sections associated with vector fields.

Process	σ [pb]	N	Process	σ [pb]	N
$W(\rightarrow \ell\nu) + \text{jets}$	35678	$2.56 \cdot 10^8$	$WW(\rightarrow 1\ell 1\nu 2\text{jets}) + \text{jets}$	24.3	$3 \cdot 10^6$
$\gamma^*/Z(\rightarrow 2\ell/2\nu) + \text{jets}$	10319	$4 \cdot 10^7$	$WW(\rightarrow 2\ell 2\nu) + \text{jets}$	5.87	$8 \cdot 10^5$
$t\bar{t}(\rightarrow 6\text{jets}) + \text{jets}$	116.2	$8 \cdot 10^6$	$WZ(\rightarrow 1\ell 1\nu 2\text{jets}) + \text{jets}$	5.03	$5 \cdot 10^5$
$t\bar{t}(\rightarrow 4\text{jets } 1\ell 1\nu) + \text{jets}$	112.4	$9 \cdot 10^6$	$WZ(\rightarrow 2\nu 2\text{jets}) + \text{jets}$	2.98	$3 \cdot 10^5$
$t\bar{t}(\rightarrow 2\text{jets } 2\ell 2\nu) + \text{jets}$	27.2	$3 \cdot 10^6$	$WZ(\rightarrow 2\ell 2\text{jets}) + \text{jets}$	1.58	$2 \cdot 10^5$
Single top + jets [<i>t</i> -channel, incl.]	87.2	$6 \cdot 10^6$	$WZ(\rightarrow 1\ell 3\nu) + \text{jets}$	1.44	$2 \cdot 10^5$
Single top + jets [<i>tW</i> -channel, incl.]	22.2	$1 \cdot 10^6$	$WZ(\rightarrow 3\ell 1\nu) + \text{jets}$	0.76	$2 \cdot 10^6$
Single top + jets [<i>s</i> -channel, incl.]	5.55	$8 \cdot 10^5$	$ZZ(\rightarrow 2\nu 2\text{jets}) + \text{jets}$	2.21	$3 \cdot 10^5$
$t\bar{t}W + \text{jets}$ [incl.]	0.25	$3 \cdot 10^4$	$ZZ(\rightarrow 2\ell 2\text{jets}) + \text{jets}$	1.18	$1.5 \cdot 10^4$
$t\bar{t}Z + \text{jets}$ [incl.]	0.21	$5 \cdot 10^4$	$ZZ(\rightarrow 4\nu) + \text{jets}$	0.63	$1 \cdot 10^5$
$t/\bar{t} + Z + j + \text{jets}$ [incl.]	0.046	$3 \cdot 10^5$	$ZZ(\rightarrow 2\nu 2\ell) + \text{jets}$	0.32	$4 \cdot 10^4$
$t\bar{t}WW + \text{jets}$ [incl.]	0.013	$2 \cdot 10^3$	$ZZ(\rightarrow 4\ell) + \text{jets}$	0.17	$4 \cdot 10^4$
$t\bar{t}t\bar{t} + \text{jets}$ [incl.]	$7 \cdot 10^{-4}$	10^3			

TABLE I. Simulated background processes given together with the related cross section σ and number of generated events N . The background contributions are split according to the massive state decays, ℓ standing equivalently for electrons, muons and taus, ν for any neutrino, and j for a jet. The notation *incl.* indicates that the sample is inclusive in the decays of the heavy particles.

Monotop production at hadron colliders can be characterized according to the decay mode of the top quark,

$$\begin{aligned}
pp &\rightarrow t + \cancel{E}_T \rightarrow bW + \cancel{E}_T \rightarrow bj\bar{j} + \cancel{E}_T, \\
pp &\rightarrow t + \cancel{E}_T \rightarrow bW + \cancel{E}_T \rightarrow b\ell + \cancel{E}_T,
\end{aligned}
\tag{2.5}$$

where j and b denote light and b -jets, respectively, ℓ a charged lepton and \cancel{E}_T missing transverse energy. In the next section, we design and investigate two search strategies associated with each of these two signatures that we dub hadronic and leptonic monotops. In both cases, we rely on the presence of a large amount of missing transverse energy carried by the invisible new state. Additionally, we base our analysis, in the hadronic case, on top quark reconstruction to reject most of the Standard Model background [12, 20], while in the leptonic case, we employ the W -boson transverse mass to maximize the signal selection efficiency and significantly reduce the background [1, 2, 7].

III. INVESTIGATING MONOTOP SIGNATURES AT THE LHC

III.1. Simulation setup

In order to investigate monotop production at the LHC, we rely on Monte Carlo simulations of the 20 fb^{-1} of collisions that have been produced during the 2012 run at a center-of-mass energy of 8 TeV. Event generation for the monotop signal relies on the implementation of the Lagrangian of Eq. (2.1) in the FEYNRULES package [21, 22] and follows the comprehensive approach for new physics proposed in Refs. [23] that links a theory to the study of its phenomenology in a straightforward fashion. We hence export the simplified theory of Section II to the UFO format [24] and make use of the MADGRAPH 5 event generator [18] to simulate parton-level events including the decays of all massive Standard Model particle. Using the QCD factorization theorem, tree-level matrix elements are convoluted in this way with the leading order set of the CTEQ6 parton density fit [19], the renormalization and factorization scales being set to the transverse mass of the produced heavy particles. Concerning the background, we directly employ the built-in Standard Model implementation of MADGRAPH 5.

Parton-level events are further integrated into a full hadronic environment by matching hard scattering matrix elements with the parton showering and hadronization infrastructure provided by the PYTHIA 6 [25] and PYTHIA 8 [26] programs for the background and new physics processes, respectively². In the case of the background, we employ the k_T -MLM prescription [27] to merge event samples described by matrix elements containing additional jets. While we

² The color structures included in the Lagrangian of Eq. (2.1) being not all fully supported by PYTHIA 6, we have employed the newer version of the program for signal event generation.

allow events associated with the production of a single gauge boson to contain up to four extra jets, this number is restricted to two for any other process. In addition, tau lepton decays possibly arising from the decays of heavier states are handled with the TAUOLA program [28] and detector effects are accounted for by using the DELPHES 2 package [29] together with the recent CMS detector description of Ref. [30]. Finally, jet reconstruction is performed with the FASTJET library [31], using an anti- k_T algorithm with a radius parameter set to $R = 0.4$ [32], and the reconstructed events are analyzed within the MADANALYSIS 5 framework [33, 34].

Background events are reweighted so that they reproduce total cross sections including higher-order corrections when available, making use in this case of the CT10 next-to-leading order (NLO) parton density fit [35] for the predictions. The values that we have used are summarized in Table I and presented together with the number of generated events, after distinguishing the different final states arising from the decays of the weak gauge bosons and top quarks. More into details, we have normalized all events originating from the production of a single gauge boson to the next-to-next-to-leading order (NNLO) accuracy [36, 37], top-antitop and single top events to the NLO one but including genuine NNLO contributions [38, 39], diboson, ttW and ttZ events to the pure NLO [40–42], while we use the leading-order results as computed by MADGRAPH 5 for all other simulated Standard Model processes. Moreover, QCD multijet contributions have been omitted as their correct treatment requires data-driven methods. We have instead chosen to resort on available experimental studies to ensure a good control of this source of background by designing appropriate event selection strategies (see the next subsections).

III.2. Hadronic monotops at the LHC

In order to probe hadronic monotops, we build an approach whose cornerstone benefits from the possible reconstruction of the hadronically decaying top quark. Event preselection involves the presence of exactly one jet tagged as originating from the fragmentation of a b -quark and two or three light jets, this last criterion allowing us to make use of monotop events featuring initial or final state radiation. This choice is motivated by an increase of the sensitivity s to monotops, s being defined as the significance $S/\sqrt{S+B}$ where S and B are respectively the number of signal and background events after all selections. The selected jet candidates are required to lie within the detector geometrical acceptance, *i.e.*, with a pseudorapidity satisfying $|\eta^j| < 2.5$, and we impose that their transverse momentum p_T is greater than 30 GeV and 50 GeV for light and b -tagged jets, respectively. Moreover, we demand that for any considered jet, the ratio between the hadronic and electromagnetic calorimeter deposits is larger than 30%. Additionally, we veto any event containing at least one identified isolated electron or muon whose transverse momentum and pseudorapidity satisfy $p_T^\ell > 10$ GeV and $|\eta^\ell| < 2.5$, respectively. We define lepton isolation on the basis of a variable I_{rel} corresponding to the amount of transverse energy, evaluated relatively to p_T^ℓ , present in a cone of radius $R = \sqrt{\Delta\varphi^2 + \Delta\eta^2} = 0.4$ centered on the lepton, φ being the azimuthal angle with respect to the beam direction. We constrain this quantity such as $I_{\text{rel}} < 20\%$.

After this preselection, we expect about $8 \cdot 10^5$ background events, although this number does not account for non-simulated multijet contributions. A good fraction of these events (35%) are issued from the production of a leptonically decaying W -boson in association with jets, the charged lepton being either too soft ($p_T^\ell < 10$ GeV), non-isolated, or lying outside the detector acceptance ($|\eta^\ell| > 2.5$). The next-to-leading background component (25% of the preselected events) is made up of top-antitop events. For half of them, both top quarks decay hadronically whereas for the other half, only one of the top quarks decays hadronically and the other one gives rise to a non-reconstructed lepton. The rest of the background finds its origin in single top production (20%), in the associated production of an invisibly-decaying Z -boson with jets (15%) while any other contribution, such as events originating from diboson or rarer Standard Model processes, is subdominant.

In addition to the presence of a single top quark, monotop signal events contain a significant amount of missing transverse energy \cancel{E}_T carried by the invisible new state. Calculating \cancel{E}_T as the norm of the sum of the transverse momenta of all the visible objects, we present on Figure 4 its distribution for the different background contributions and a few representative signal scenarios. On the left panel of the figure, we focus on scenarios of class **SI** where the monotop state arises from a flavor-changing neutral interaction. We consider lighter scalar invisible particles (**SI.s** scenarios) with $m_\phi = 100$ GeV and $m_\phi = 300$ GeV and heavier vector invisible particles (**SI.v** scenarios) with $m_V = 600$ GeV and $m_V = 1000$ GeV. Each signal distribution exhibits a peak whose position depends on the invisible particle mass and a tail extending, with a gently decreasing slope, to missing transverse energy values larger than 500 GeV. For new states heavier than about 100 GeV, few signal events are expected in the parameter space region where the bulk of the Standard Model events lies, so that a key requirement on the missing transverse energy would simultaneously allow for a good background rejection and an important signal selection efficiency.

On the right panel of Figure 4, we consider four representative **SII** scenarios where the monotop signature arises from the decay of a colored resonance. Two of these feature a heavy scalar resonant state of mass $m_\varphi = 1000$ GeV (**SII.s** scenarios) and a monotop system constituted of a top quark and an invisible fermion being either quite light

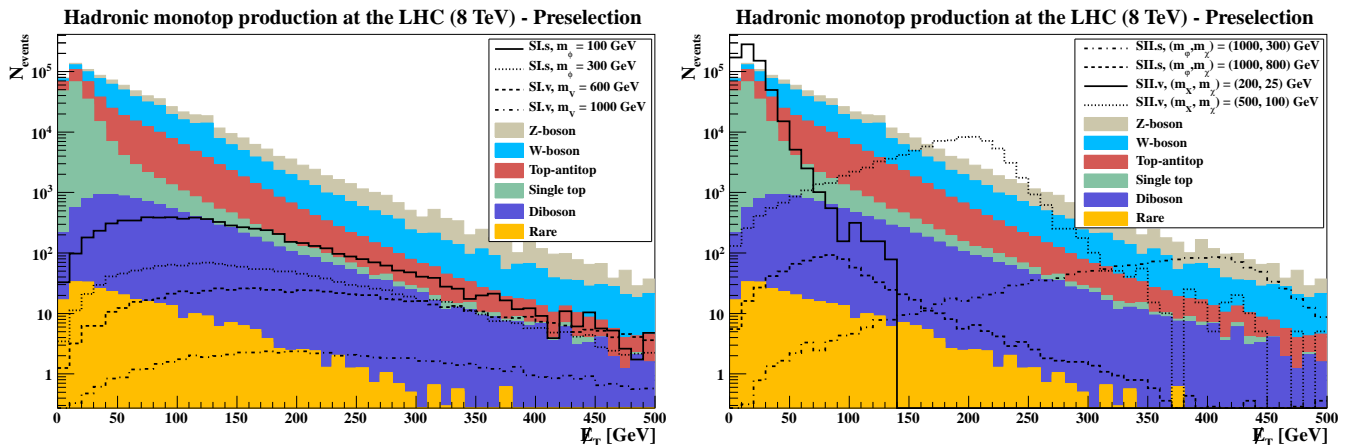


FIG. 4. Missing transverse energy distributions after preselecting events with one single b -tagged jet, two or three light jets and no isolated electron or muon. We represent separately (and stacked) the various contributions to the Standard Model expectation, to which we superimpose predictions for eight representative signal scenarios of class **SI** (left panel) and **SII** (right panel), the new physics coupling strengths being each time fixed to $a = 0.1$.

($m_\chi = 300$ GeV) or rather heavy ($m_\chi = 800$ GeV). In the first case, the available phase space for the resonance decay is important while in the second case, the monopole state has to be produced almost at threshold. The last two scenarios focus on vector resonances (type **SII.v**). For one of them, the resonant state is rather light ($m_X = 200$ GeV) and the mass of the invisible fermion is fixed to $m_\chi = 25$ GeV, while for the other one, the resonance is heavier ($m_X = 500$ GeV) and the invisible state is still moderately light ($m_\chi = 100$ GeV). All missing transverse energy distributions present a typical resonant behavior with an edge, distorted due to detector effects, at a \cancel{E}_T value depending both on the resonance and invisible particle masses. When the monopole system has to be produced close to threshold, monopole events are not expected to contain a large quantity of missing transverse energy so that any \cancel{E}_T requirement with a good Standard Model background rejection has consequently a poor signal efficiency. When the mass difference between the two new states increases, the edge of the \cancel{E}_T spectrum moves to larger values so that the sensitivity to such scenarios is expected to be more important.

From those considerations, we design two different hadronic monopole search strategies. The first one is dedicated to the low mass region of the parameter space with a lower selection threshold on the missing transverse energy, whereas the second one is based on a harder selection more sensible to the high mass region. We choose

$$\text{either } \cancel{E}_T > 150 \text{ GeV} \quad \text{or} \quad \cancel{E}_T > 250 \text{ GeV} . \quad (3.1)$$

Such requirements on the missing transverse energy, together with the current preselection criteria on jets, are also expected to imply a good control of the non-simulated multijet background [12, 43, 44]. After imposing the looser $\cancel{E}_T > 150$ GeV criterion³, about 45000 background events survive and are mostly consisting of events related to the production of an invisibly decaying Z -boson (43%), a W -boson (37%) or a top-antitop pair (15%) with jets. With the tighter missing transverse energy requirement $\cancel{E}_T > 250$ GeV, most of the Standard Model background is rejected and only about 8000 events, originating from the production of a Z -boson (53%), a W -boson (33%) or a top-antitop pair (8%) in association with jets, remain.

The next steps of the selection strategy are based on the top quark reconstruction from the final state jets and on the kinematical configuration of the signal events, the missing transverse momentum and the reconstructed top quark being mainly back-to-back. Two of the selected light jets j_1 and j_2 are hence imposed to have an invariant mass $M_{j_1 j_2}$ compatible with the mass of a W -boson,

$$M_{j_1 j_2} \in]50, 105[\text{ GeV} . \quad (3.2)$$

In the case of events with three selected light jets, $M_{j_1 j_2}$ is defined as the invariant mass of the dijet system whose invariant mass is the closest to the W -boson mass. In addition, we require the two-momentum of the leading jet $\vec{p}(j_1)$

³ Such a low missing transverse energy requirement might however be challenging with respect to \cancel{E}_T -only trigger efficiencies in the context of a real experiment.

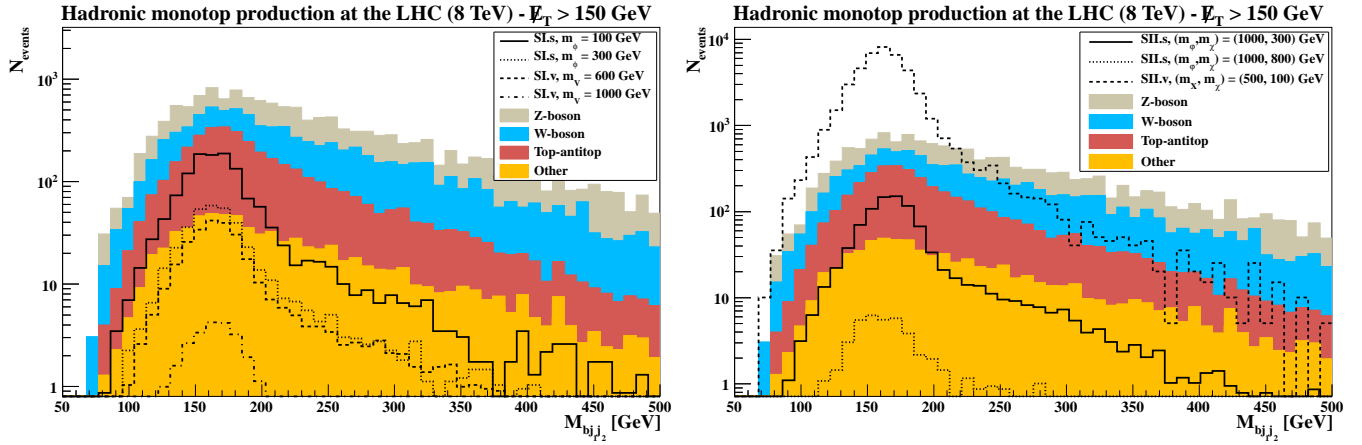


FIG. 5. Invariant mass distribution of the reconstructed top quark after all requirements described in the text and a loose missing transverse energy selection of $\cancel{E}_T > 150$ GeV. We present separately (and stacked) the various contributions to the Standard Model expectation to which we superimpose predictions for eight representative signal scenarios of class **SI** (left panel) and **SII** (right panel), the coupling strengths being fixed to $a = 0.1$.

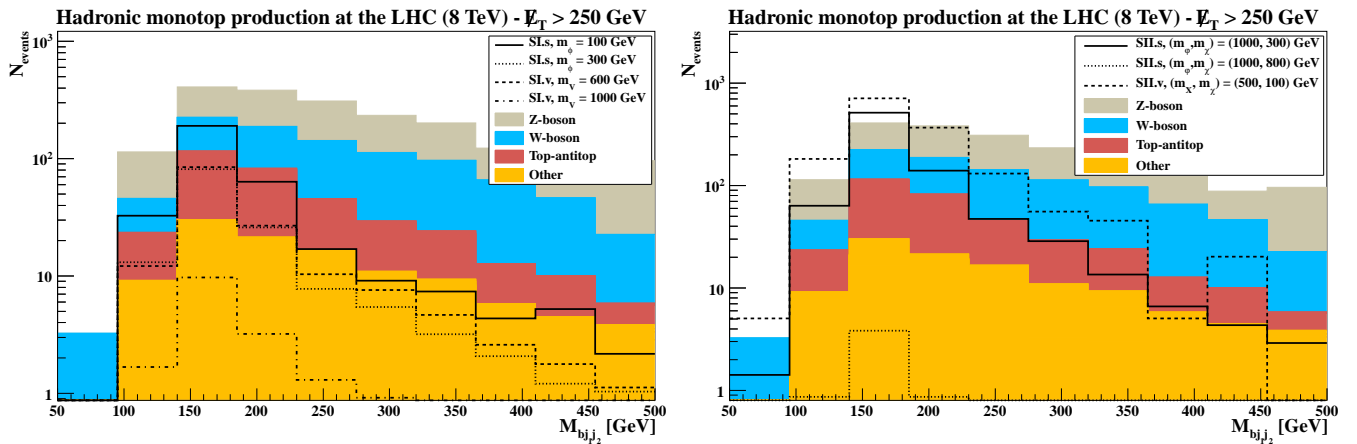


FIG. 6. Same as in Figure 5 but for a missing transverse energy requirement of $\cancel{E}_T > 250$ GeV.

to be non-collinear with the missing transverse momentum $\vec{\cancel{p}}_T$ defined as the opposite of the sum of the transverse momenta of all visible objects,

$$\Delta\varphi(\vec{\cancel{p}}_T, \vec{p}(j_1)) \in]0.5, 5.75[. \quad (3.3)$$

Taking into account the selected b -tagged jet, we fully reconstruct the top quark and demand that its two-momentum $\vec{p}(t)$ is well separated from the missing two-momentum,

$$\Delta\varphi(\vec{\cancel{p}}_T, \vec{p}(t)) \in]1, 5[. \quad (3.4)$$

At this stage of the analysis, the background is comprised of about 15000 (2000) events when one imposes that $\cancel{E}_T > 150$ GeV (250 GeV), composed of 40% (52%), 33% (31%) and 22% (11%) of events related to the production of a Z -boson, a W -boson and a top-antitop pair, respectively. The results of the two analysis strategies are illustrated on Figure 5 (loose \cancel{E}_T requirement) and Figure 6 (tight \cancel{E}_T requirement) where we present the spectrum in the invariant mass of the reconstructed top quark $M_{bj_1j_2}$ for the dominant background contributions and a few representative signal scenarios of class **SI** (left panel of the figures) and **SII** (right panel of the figures). Since the bulk of signal events are populating bins with a value around the top mass with a narrower spread than for the background, whose spectrum also exhibits a continuum extending to larger $M_{bj_1j_2}$ values, we enforce

$$M_{bj_1j_2} \in]140, 195[\text{ GeV}. \quad (3.5)$$

Process	$N_{ev}, \cancel{E}_T > 150 \text{ GeV}$	$N_{ev}, \cancel{E}_T > 250 \text{ GeV}$
Z-boson production	1411 ± 38	210 ± 15
W-boson production	1064 ± 33	148 ± 12
Top-antitop pair production	1486 ± 39	105 ± 10
Other background contributions	262 ± 15	34.7 ± 5.9
Total background	4223 ± 65	497 ± 22
SI.s , $m_\phi = 100 \text{ GeV}$	885 ± 29	212 ± 15
SI.s , $m_\phi = 300 \text{ GeV}$	268 ± 16	92.0 ± 9.5
SI.v , $m_V = 600 \text{ GeV}$	191 ± 14	95.6 ± 9.7
SI.v , $m_V = 1000 \text{ GeV}$	19.7 ± 4.3	11.0 ± 3.3
SII.s , $m_\phi = 1000 \text{ GeV}$, $m_\chi = 300 \text{ GeV}$	664 ± 25	581 ± 23
SII.s , $m_\phi = 1000 \text{ GeV}$, $m_\chi = 800 \text{ GeV}$	29.4 ± 5.4	4.1 ± 2.0
SII.v , $m_X = 200 \text{ GeV}$, $m_\chi = 25 \text{ GeV}$	≈ 0	≈ 0
SII.v , $m_X = 500 \text{ GeV}$, $m_\chi = 100 \text{ GeV}$	31047 ± 171	334 ± 18

TABLE II. Number of expected events (N_{ev}), after applying all the selections described in the text, for 20 fb^{-1} of LHC collisions at a center-of-mass energy of 8 TeV, given together with the associated statistical uncertainties. We present separately the different contributions to the Standard Model background and results for the eight representative signal scenarios introduced in this section. The new physics coupling parameter is set to $a = 0.1$.

This allows for a good signal selection efficiency and an important rejection of the background contamination.

Considering a new physics coupling set to $a = 0.1^4$ and 20 fb^{-1} of LHC collisions at a center-of-mass energy of 8 TeV, the number of events surviving all selections are given in Table II, for the different background contributions and the series of signal scenarios investigated so far. While flavor-changing monotop production (scenarios of class **SI**) predicts a number of surviving events depending only on the invisible particle mass (and on the value of the a parameter), resonant scenarios (of class **SII**) lead to a number of selected events depending on both the resonant mass, whose monotop production cross section depends on (together with the coupling parameter), and on its difference with the sum of the top and the invisible fermion mass controlling the position of the edge in the missing transverse energy distribution. The numbers of selected signal (S) and background (B) events can be subsequently reexpressed in terms of the LHC sensitivity, that we define as the significance $s = S/\sqrt{S+B}$, to hadronic monotops. The dependence of the s quantity on the model parameters is presented in (m_ϕ, a) and (m_V, a) planes for scenarios of class **SI.s** and **SI.v** on the left and right panels of Figure 7, respectively, and in (m_χ, m_ϕ) and (m_χ, m_X) planes for scenarios of class **SII.s** and **SII.v** (considering several fixed values of the a parameter) on the left and right panels of Figure 8. We indicate the contour lines associated with $s = 3$ (dotted curves) and $s = 5$ (plain curves) related to a 3σ observation or a 5σ discovery of a monotop hint at the LHC.

It turns out that the LHC is more sensitive to scenarios involving vector states, an effect directly related to the larger associated cross sections compared to the scalar cases. Next, it is found that models with larger or moderate couplings of about $a \gtrsim 0.1$ are well covered by both developed search strategies, so that new physics masses ranging up to 2 TeV are foreseen to be observable at the LHC in the most optimistic cases. The reaches are reduced in the case of models with a smaller coupling strength, although the LHC still remains a promising machine for accessing the low mass regions of the parameter space. In each case, we present results associated with the \cancel{E}_T requirement giving rise to the best sensitivity, *i.e.*, with the loose criterion ($\cancel{E}_T < 150 \text{ GeV}$) for flavor-changing monotop production and the tight one ($\cancel{E}_T < 250 \text{ GeV}$) for resonant production. Generally, the larger missing transverse energy requirement increases, compared to the looser \cancel{E}_T selection, the sensitivity to the high mass parameter space regions whereas it simultaneously decreases the one to the low mass regions.

Finally, we recall that monotop production induced by a flavor-changing interaction has been recently searched for by the CDF collaboration at the Tevatron in the context of scenarios where the invisible particle is a new vector state [17]. It has been found that for a coupling strength of $a = 0.1$, benchmark scenarios for which $m_V < 140 \text{ GeV}$ have been excluded by data. From the results of Figure 7, we conclude that future LHC searches for monotops are able to greatly improve these current constraints.

⁴ Results for other values of a can be easily deduced as the number of selected signal events is proportional to a^2 .

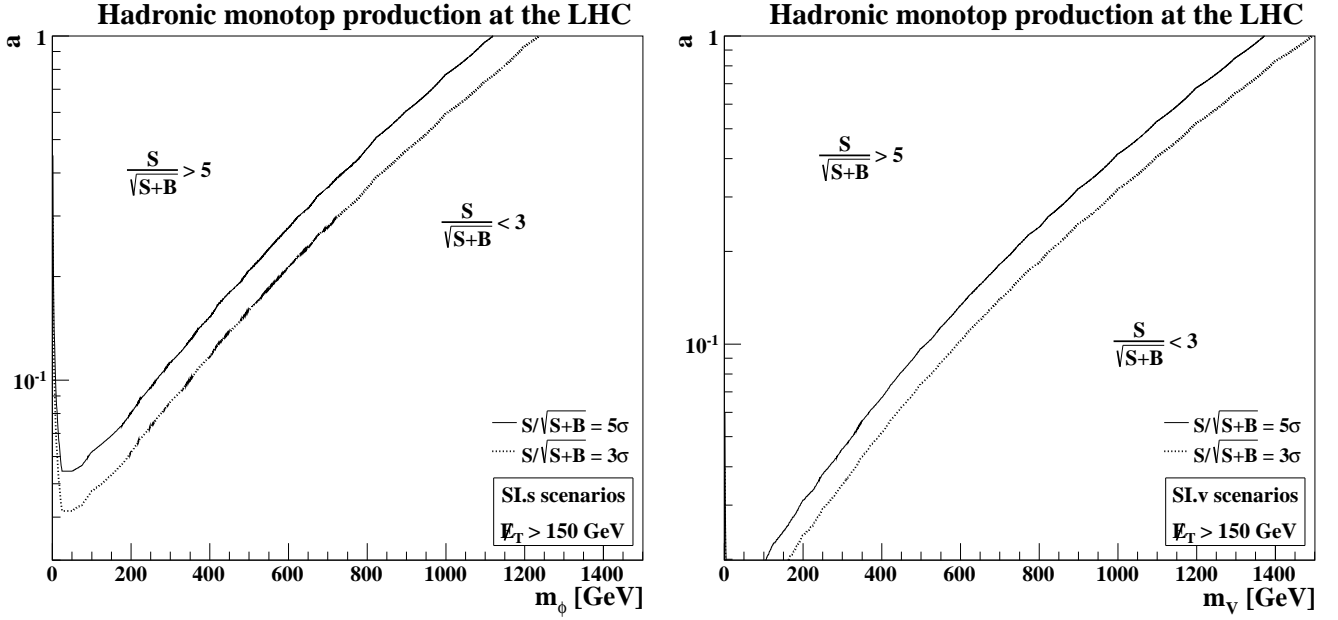


FIG. 7. LHC sensitivity to hadronic monotop production in the context of scenarios of class **SI** where the Standard Model is supplemented by a scalar (left panel) or vector (right panel) invisible particle, for 20 fb^{-1} of proton-proton collisions at a center-of-mass energy of 8 TeV. The sensitivity is calculated as the ratio $S/\sqrt{S+B}$ where S and B are the number of signal and background events surviving all selections presented in the text. The results are given in (m_ϕ, a) and (m_v, a) planes for scenarios of class **SI.s** and **SI.v**, respectively, and we focus on the loose \cancel{E}_T requirement which leads to better sensitivity in the case of **SI** scenarios.

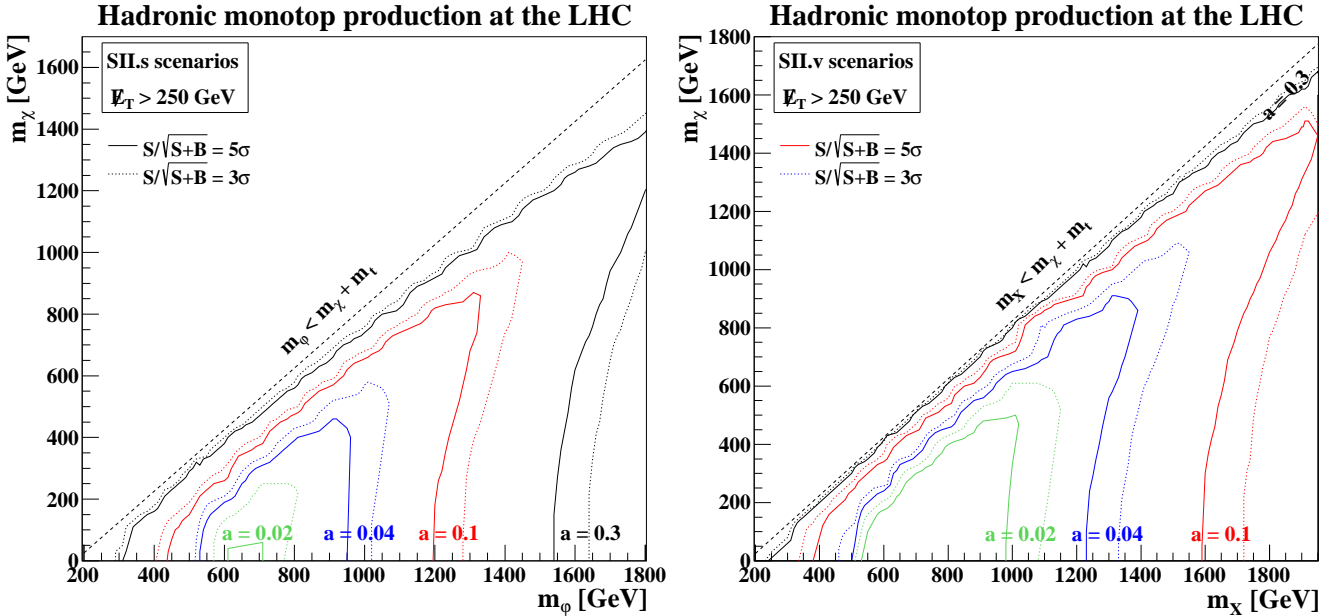


FIG. 8. Same as Figure 7 but for scenarios of type **SII**. The results are given in (m_χ, m_ϕ) and (m_χ, m_X) planes for scenarios of class **SII.s** (left panel) and **SII.v** (right panel), respectively, and presented for several values of the coupling parameter $a = 0.02$ (green), 0.04 (blue), 0.1 (red) and 0.3 (black). We focus on the tight \cancel{E}_T requirement which leads to better sensitivity in the case of **SII** scenarios and the regions below the plain and dashed lines are excluded at the 5σ and 3σ levels, respectively.

III.3. Leptonic monotops at the LHC

Hadronic monotops have received special attention in the past as the associated signature offers the possibility to use top reconstruction as a tool for background rejection. In contrast, the leptonic mode is believed to be more challenging since the branching fraction of the top quark into a leptonic state is smaller and since there are two different sources of missing transverse energy, namely a neutrino arising from the top quark leptonic decay and the new invisible state. However, we choose, in this work, to be pragmatic and focus on both the hadronic and leptonic channels. First, the possibility of using leptonic triggers in the context of the LHC experiments offers a mean to increase the sensitivity to parameter space regions implying events with a smaller quantity of missing transverse energy or a smaller cross section. Next, both channels are complementary and statistically independent, which offers ways for further improvements of the obtained limits by combining the results. Finally, the hadronic channel is associated with large systematic uncertainties due, on the one hand, to the jet energy scale, and, on the other hand, to the modeling and the resolution of the missing transverse energy. These two sources of uncertainties are however less critical in the leptonic case, which provides a further motivation for studying this case.

Event preselection is based on the expected particle content of final states associated with the signal. We hence require the presence of exactly one hard and isolated electron or muon. Its transverse-momentum is demanded to fulfill $p_T^\ell > 30$ GeV and its pseudorapidity to be compatible with the CMS detector geometrical acceptance $|\eta^\ell| < 2.5$. Lepton isolation is defined differently from the choice of Section III.2 since leptons are used here to define the signal region and not to veto background events. We compute a variable I'_{rel} where the amount of transverse energy present in a cone of $R = 0.3$, and not $R = 0.4$ as in the hadronic case, is calculated relatively to the lepton transverse momentum. The significance s of a monotop signature is found increased when we ask for $I'_{\text{rel}} < 0.18$ and $I'_{\text{rel}} < 0.06$ for electrons and muons, respectively, a result largely holding for most of the reachable parameter space. In principle, jets or leptons originating from the fragmentation of a heavy quark can be misidentified as an isolated hard lepton. However, our detector simulation framework does not account for jets faking leptons, so that the total ‘fake’ contribution to the background is clearly not correctly modeled in our analysis. Although we have neglected this source of background, recent ATLAS and CMS measurements of the single-top cross section in the t -channel production mode have shown that selection criteria compatible with those introduced below allow us to make it under good control [45, 46]. Additionally, the missing transverse energy requirements that are imposed (see below) are tighter than the one employed in the single top analyses, which further reduces the fake contamination that is besides driven by QCD multijet subprocesses.

An overwhelming Standard Model background consisting of about $2 \cdot 10^8$ events is expected to pass this selection criterion. It mainly finds its origin in the production of a leptonically decaying W -boson with jets (91% of the background) or of a Z -boson with jets (8% of the background) where one of the produced leptons is non-reconstructed. Other background processes such as top-antitop pair, single top and diboson production are all contributing in a much smaller extent (below 1%).

In the next selection requirement, we make use of the configuration of the signal final state which features a b -tagged jet. We then enforce the presence, within the selected events, of one single b -tagged jet lying within the detector acceptance ($|\eta^j| < 2.5$) and with a large transverse momentum $p_T^j > 75$ GeV. This last criterion has been optimized to allow for a good background rejection over most of the parameter space and finds its source in the fact that signal jets can be rather hard as issued from a top quark decay whilst jets accompanying a singly-produced gauge boson are in general much softer as arising from initial state radiation. In addition, events exhibiting the presence of any other jet with a transverse momentum larger than 20 GeV are vetoed, so that the (already subdominant) contamination by single top and top-antitop events is further reduced. These two selections allow to reduce the number of surviving background events which are consisting of W -boson and Z -boson in 88% and 10% of the cases by a factor of more than 700.

As stated above, the missing transverse energy present in events describing the production of a leptonically decaying monotop system arises from two sources, the neutrino issued from the decay of the top quark and the invisible new state, in contrast to Standard Model events where the \cancel{E}_T is only originating from neutrinos or misreconstruction effects. We benefit from this property to estimate the W -boson transverse mass M_T^W obtained when considering that all the missing transverse energy finds its origin in a W -boson decay,

$$M_T^W = \sqrt{2p_T^\ell \cancel{E}_T \left[1 - \cos \Delta\phi_{\ell, \cancel{E}_T} \right]}, \quad (3.6)$$

where $\Delta\phi_{\ell, \cancel{E}_T}$ stands for the angular distance, in the azimuthal direction with respect to the beam, between the lepton and the missing transverse energy. As the dominant Standard Model contribution is described by events where a real W -boson can be reconstructed, the M_T^W distribution of the background is expected to peak at smaller M_T^W values, contrary to the signal. This is illustrated on Figure 9 where we superimpose to the background expectation predictions for the eight signal scenarios introduced in Section III.2, one of them being already invisible at that stage.

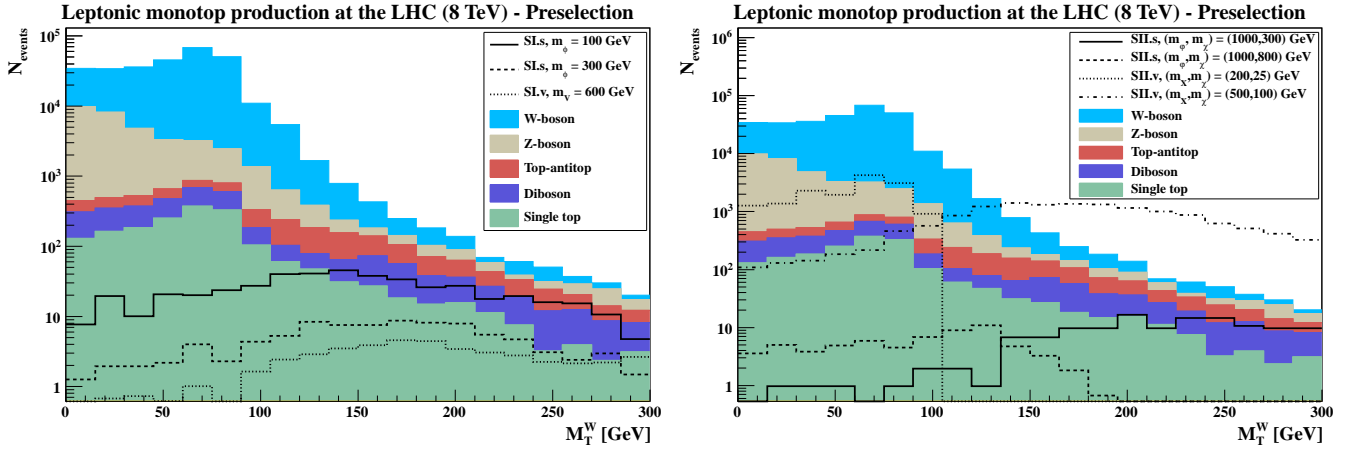


FIG. 9. W -boson transverse mass spectrum after selecting events with one single b -tagged jet and one single lepton as described in the text. We present separately (and stacked) the various contributions to the Standard Model expectation to which we superimpose predictions for seven of the eight representative signal scenarios of section III.2.

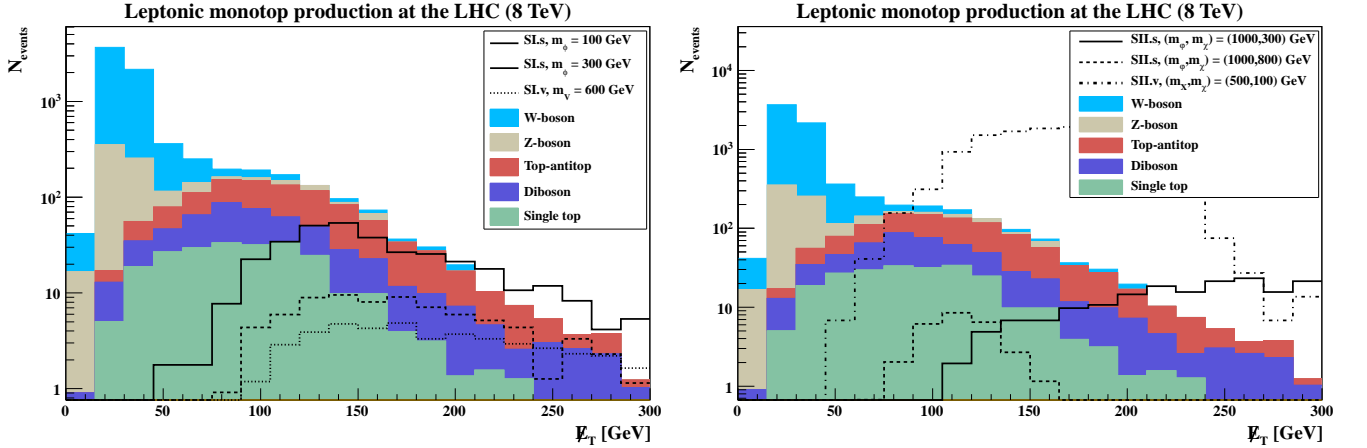


FIG. 10. Missing transverse energy distributions after selecting events with one single b -tagged jet, one single lepton and the requirement on the W -boson transverse mass described in the text. We present separately (and stacked) the various contributions to the Standard Model expectation to which we superimpose predictions for the eight representative signal scenarios of Section III.2.

In the case of flavor-changing monotop production, the signal spectra are very broad and extend to very large M_T^W values. In contrast, monotop production induced by the decay of a colored resonance imply distributions that present an edge distorted by detector effects whose position depends on the resonance and invisible particle masses. In order to increase the sensitivity to most monotop benchmark scenarios, we require

$$M_T^W > 115 \text{ GeV} . \quad (3.7)$$

This reduces the background by an extra factor of 40 so that we expect that about 4000 background events survive, the latter being constituted of events issued from W -boson (77%), Z -boson (9%), top-antitop (7%), diboson (4%) and single top (3%) production in association with jets. In addition, such a selection on the W -boson transverse mass has also the advantage to render the non-simulated multijet background under good control [47, 48].

The results of the analysis strategy above are further depicted on Figure 10 where we present the missing transverse energy distribution for the different sources of Standard Model background, together with predictions for the eight monotop benchmark scenarios introduced in Section III.2, two of them turning out to be invisible after the M_T^W selection. While the bulk of the Standard Model background events lie well within the low missing transverse energy region, events originating from the considered signal scenarios are exhibiting peaks whose maximum position lies in general around larger E_T values, their magnitude depending strongly on the benchmark model. Furthermore, monotop E_T spectra also extend to very large E_T values. In contrast to the hadronic analysis where we can employ

Process	$N_{ev}, \cancel{E}_T > 120 \text{ GeV}$	$N_{ev}, \cancel{E}_T > 162 \text{ GeV}$	$N_{ev}, \cancel{E}_T > 204 \text{ GeV}$	$N_{ev}, \cancel{E}_T > 225 \text{ GeV}$
Top-antitop pair production	237 ± 15	76.94 ± 8.77	22.70 ± 4.76	11.77 ± 3.43
W -boson production	27.85 ± 5.28	8.35 ± 2.89	≈ 0	≈ 0
Diboson production	95.78 ± 9.79	40.18 ± 6.34	18.63 ± 4.32	13.32 ± 3.65
Single top production	62.45 ± 7.90	14.46 ± 3.80	5.08 ± 2.25	3.13 ± 1.77
Z -boson production	36.71 ± 6.06	5.24 ± 2.29	≈ 0	≈ 0
Other background contributions	0.39 ± 0.62	0.29 ± 0.53	0.19 ± 0.43	0.10 ± 0.31
Total background	460 ± 21	145 ± 12	46.60 ± 6.83	28.32 ± 5.32
SI.s , $m_\phi = 100 \text{ GeV}$	300 ± 17	-	-	-
SI.s , $m_\phi = 300 \text{ GeV}$	-	50.41 ± 7.10	-	-
SI.v , $m_V = 600 \text{ GeV}$	-	-	28.01 ± 5.29	-
SI.v , $m_V = 1000 \text{ GeV}$	-	-	-	2.64 ± 1.62

Process	$N_{ev}, \cancel{E}_T > 192 \text{ GeV}$	$N_{ev}, \cancel{E}_T > 90 \text{ GeV}$	$N_{ev}, \cancel{E}_T > 0 \text{ GeV}$	$N_{ev}, \cancel{E}_T > 90 \text{ GeV}$
Top-antitop pair production	33.85 ± 5.82	379 ± 19	536 ± 23	379 ± 19
W -boson production	2.78 ± 1.67	80.75 ± 8.99	5720 ± 76	80.75 ± 8.99
Diboson production	23.79 ± 4.88	174 ± 13	297 ± 17	174 ± 13
Single top production	7.04 ± 2.65	129 ± 11	236 ± 15	129 ± 11
Z -boson production	≈ 0	62.93 ± 7.93	687 ± 26	62.93 ± 7.93
Other background contributions	0.28 ± 0.53	0.57 ± 0.75	0.66 ± 0.81	0.57 ± 0.75
Total background	67.74 ± 8.23	826 ± 29	7476 ± 86	826 ± 29
SII.s , $(m_\phi, m_\chi) = (1000, 300) \text{ GeV}$	269 ± 16	-	-	-
SII.s , $(m_\phi, m_\chi) = (1000, 800) \text{ GeV}$	-	26.48 ± 5.15	-	-
SII.v , $(m_X, m_\chi) = (200, 25) \text{ GeV}$	-	-	≈ 0	-
SII.v , $(m_X, m_\chi) = (500, 100) \text{ GeV}$	-	-	-	12381 ± 111

TABLE III. Number of events (N_{ev}) expected after applying all the selections described in the text, for 20 fb^{-1} of LHC collisions at a center-of-mass energy of 8 TeV, given together with the associated statistical uncertainties. We present separately the different contributions to the Standard Model background and results for the eight representative signal scenarios considered in this work. The new physics coupling parameter a is set to 0.1 and the value of the optimized missing transverse energy selection is also indicated.

top reconstruction to enhance the signal over background ratio, no such possibility is available in the leptonic case. Therefore, in order to get reasonable significance over the entire parameter space, we choose to optimize the missing transverse energy selection criterion for each given benchmark scenario so that the quantity s defined as above, *i.e.*, $s = S/\sqrt{S+B}$, S and B being respectively the number of selected signal and background events after all the selection steps, is maximized.

We present on Table III the number of remaining events after all selections for the different contributions to the Standard Model background as well as for the eight monotop scenarios of Section III.2. Our predictions are normalized to 20 fb^{-1} of LHC collisions at a center-of-mass energy of 8 TeV and in each case, we include the derived value for the optimized missing transverse energy requirement. When the monotop state is produced via a flavor-changing neutral interaction and for a new physics coupling strength of $a = 0.1$, the number of expected signal events is in general relatively large when compared to the background expectation, at least for invisible masses below 600 GeV. Consequently, we expect that an important fraction of the monotop parameter space for scenarios of class **SI** can be reachable with the available integrated luminosity for collisions at $\sqrt{S_h} = 8 \text{ TeV}$. This is illustrated on Figure 11 where we present, in (m_ϕ, a) (left panel of the figure) and (m_V, a) (right panel of the figure) planes contours associated with a 3σ and 5σ significance for scenarios of class **SI.s** and **SI.v**, respectively. The results are found to be comparable to the hadronic case, although the sensitivity to the larger mass regions of the parameter space is slightly increased. In the second part of the table and on Figure 12, we turn to the investigation of the LHC sensitivity to the resonant production of leptonically decaying monotops. We again obtain conclusions similar to the hadronic case with a slight increase in sensitivity for the high mass region of the parameter space, as shown in the (m_χ, m_ϕ) and (m_χ, m_X) planes of scenarios of class **SII.s** and **SII.v** (considering several fixed values of the a parameter) on the left and right panels of Figure 12.

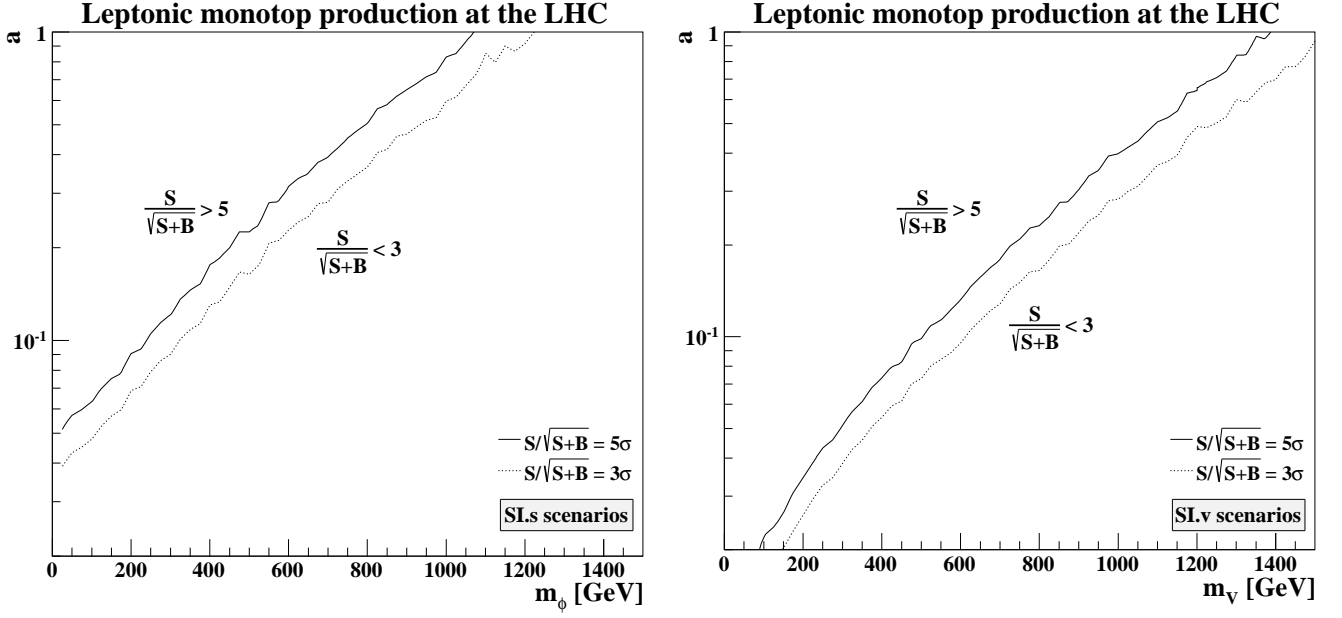


FIG. 11. LHC sensitivity to leptonic monotop production in the context of scenarios of class **SI** where the Standard Model is supplemented by a scalar (left panel) or vector (right panel) invisible particle, for 20 fb^{-1} of proton-proton collisions at a center-of-mass energy of 8 TeV. The sensitivity is calculated as the ratio $S/\sqrt{S+B}$ where S and B are the number of signal and background events surviving all selections presented in the text. The results are given in (m_ϕ, a) and (m_V, a) planes for scenarios of class **SI.s** and **SI.v**, respectively.

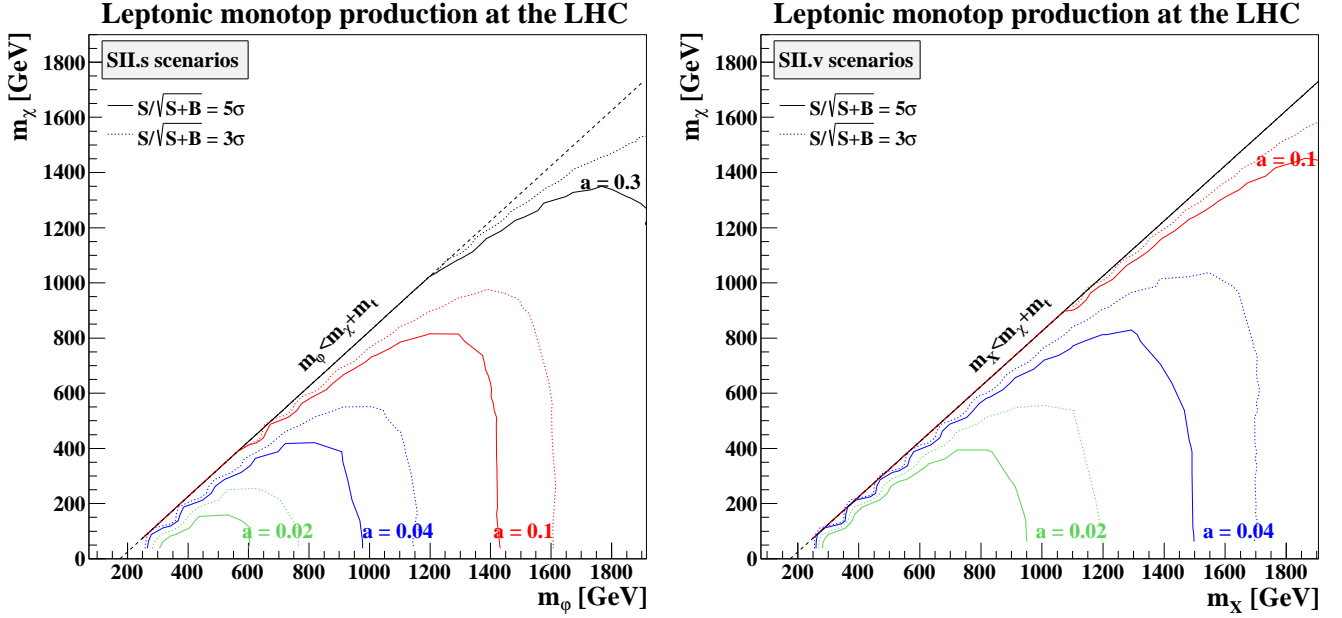


FIG. 12. Same as Figure 11 but for scenarios of type **SII**. The results are given in (m_χ, m_ϕ) and (m_χ, m_X) planes for scenarios of class **SII.s** (left panel) and **SII.v** (right panel), respectively, and presented for several values of the coupling parameter $a = 0.02$ (green), 0.04 (blue), 0.1 (red) and 0.3 (black). The regions below the plain and dashed lines are excluded at the 5σ and 3σ levels, respectively.

IV. CONCLUSIONS

In this paper, we have investigated in details the LHC phenomenology of the monotop signature. We have considered a set of representative scenarios based on a simplified model description that feature all the possible production modes of a monotop state at a hadronic collider. It has been shown that, by means of state-of-the-art Monte Carlo simulations including a modeling of a CMS-like detector response of the 20 fb^{-1} of collisions that have been produced at the 2012 LHC run at a center-of-mass energy of 8 TeV, a large fraction of the parameter space is in principle reachable. In our work, we have followed a pragmatic approach and studied both the hadronic and leptonic decay modes of the monotop system, even though the last case might be naively thought as more challenging to observe. We have designed several dedicated analyses allowing to derive the new physics masses and couplings that are observable at the 3σ and 5σ level. In particular and for couplings of about $a = 0.1$, masses ranging up to 300 GeV (500 GeV) could be observed when the monotop state is produced via flavor-changing neutral interactions with a new scalar (vector) state. In contrast, monotop resonant production allows to access beyond the Standard Model masses ranging up to about 1 TeV (1.5 TeV) when the Standard Model contains a new scalar (vector) colored field. Those results are very encouraging and should motivate further investigations by both the ATLAS and CMS experiments in the context of real data.

ACKNOWLEDGMENTS

The authors are grateful to K. Kotov for lively discussions on the topic. This work has been partially supported by the Theory-LHC France-initiative of the CNRS/IN2P3, by the French ANR 12 JS05 002 01 BATS@LHC and by a Ph.D. fellowship of the French ministry for education and research.

-
- [1] Edmond L. Berger, B.W. Harris, and Z. Sullivan, “Single top squark production via R-parity violating supersymmetric couplings in hadron collisions,” *Phys.Rev.Lett.* **83**, 4472–4475 (1999), [arXiv:hep-ph/9903549 \[hep-ph\]](#).
 - [2] Edmond L. Berger, B.W. Harris, and Z. Sullivan, “Direct probes of R-parity violating supersymmetric couplings via single top squark production,” *Phys.Rev.* **D63**, 115001 (2001), [arXiv:hep-ph/0012184 \[hep-ph\]](#).
 - [3] Nishita Desai and Biswarup Mukhopadhyaya, “R-parity violating resonant stop production at the Large Hadron Collider,” *JHEP* **1010**, 060 (2010), [arXiv:1002.2339 \[hep-ph\]](#).
 - [4] Abhishek Kumar, John N. Ng, Andrew Spray, and Peter T. Winslow, “Tracking Down the Top Quark Forward-Backward Asymmetry with Monotops,” *Phys.Rev.* **D88**, 075012 (2013), [arXiv:1308.3712 \[hep-ph\]](#).
 - [5] Hooman Davoudiasl, David E. Morrissey, Kris Sigurdson, and Sean Tulin, “Baryon Destruction by Asymmetric Dark Matter,” *Phys.Rev.* **D84**, 096008 (2011), [arXiv:1106.4320 \[hep-ph\]](#).
 - [6] Jernej F. Kamenik and Jure Zupan, “Discovering Dark Matter Through Flavor Violation at the LHC,” *Phys.Rev.* **D84**, 111502 (2011), [arXiv:1107.0623 \[hep-ph\]](#).
 - [7] Ezequiel Alvarez, Estefania Coluccio Leskow, Jure Drobnak, and Jernej F. Kamenik, “Leptonic Monotops at LHC,” (2013), [arXiv:1310.7600 \[hep-ph\]](#).
 - [8] Jian Wang, Chong Sheng Li, Ding Yu Shao, and Hao Zhang, “Search for the signal of monotop production at the early LHC,” *Phys.Rev.* **D86**, 034008 (2012), [arXiv:1109.5963 \[hep-ph\]](#).
 - [9] D.E. Morrissey, Timothy M.P. Tait, and C.E.M. Wagner, “Proton lifetime and baryon number violating signatures at the CERN LHC in gauge extended models,” *Phys.Rev.* **D72**, 095003 (2005), [arXiv:hep-ph/0508123 \[hep-ph\]](#).
 - [10] Zhe Dong, Gauthier Durieux, Jean-Marc Gerard, Tao Han, and Fabio Maltoni, “Baryon number violation at the LHC: the top option,” *Phys.Rev.* **D85**, 016006 (2012), [arXiv:1107.3805 \[hep-ph\]](#).
 - [11] F. del Aguila, J.A. Aguilar-Saavedra, and L. Ametller, “Z t and gamma t production via top flavor changing neutral couplings at the Fermilab Tevatron,” *Phys.Lett.* **B462**, 310–318 (1999), [arXiv:hep-ph/9906462 \[hep-ph\]](#).
 - [12] J. Andrea, B. Fuks, and F. Maltoni, “Monotops at the LHC,” *Phys.Rev.* **D84**, 074025 (2011), [arXiv:1106.6199 \[hep-ph\]](#).
 - [13] R. Bernabei *et al.* (DAMA Collaboration), “First results from DAMA/LIBRA and the combined results with DAMA/NaI,” *Eur.Phys.J.* **C56**, 333–355 (2008), [arXiv:0804.2741 \[astro-ph\]](#).
 - [14] C.E. Aalseth *et al.* (CoGeNT collaboration), “Results from a Search for Light-Mass Dark Matter with a P-type Point Contact Germanium Detector,” *Phys.Rev.Lett.* **106**, 131301 (2011), [arXiv:1002.4703 \[astro-ph.CO\]](#).
 - [15] C.E. Aalseth, P.S. Barbeau, J. Colaresi, J.I. Collar, J. Diaz Leon, *et al.*, “Search for an Annual Modulation in a P-type Point Contact Germanium Dark Matter Detector,” *Phys.Rev.Lett.* **107**, 141301 (2011), [arXiv:1106.0650 \[astro-ph.CO\]](#).
 - [16] G. Angloher, M. Bauer, I. Bavykina, A. Bento, C. Bucci, *et al.*, “Results from 730 kg days of the CRESST-II Dark Matter Search,” *Eur.Phys.J.* **C72**, 1971 (2012), [arXiv:1109.0702 \[astro-ph.CO\]](#).
 - [17] T. Aaltonen *et al.* (CDF Collaboration), “Search for a dark matter candidate produced in association with a single top quark in $p\bar{p}$ collisions at $\sqrt{s} = 1.96 \text{ TeV}$,” *Phys.Rev.Lett.* **108**, 201802 (2012), [arXiv:1202.5653 \[hep-ex\]](#).

- [18] Johan Alwall, Michel Herquet, Fabio Maltoni, Olivier Mattelaer, and Tim Stelzer, “MadGraph 5 : Going Beyond,” *JHEP* **1106**, 128 (2011), [arXiv:1106.0522 \[hep-ph\]](#).
- [19] J. Pumplin, D.R. Stump, J. Huston, H.L. Lai, Pavel M. Nadolsky, *et al.*, “New generation of parton distributions with uncertainties from global QCD analysis,” *JHEP* **0207**, 012 (2002), [arXiv:hep-ph/0201195 \[hep-ph\]](#).
- [20] Benjamin Fuks, “Beyond the Minimal Supersymmetric Standard Model: from theory to phenomenology,” *Int.J.Mod.Phys. A* **27**, 1230007 (2012), [arXiv:1202.4769 \[hep-ph\]](#).
- [21] Neil D. Christensen and Claude Duhr, “FeynRules - Feynman rules made easy,” *Comput.Phys.Commun.* **180**, 1614–1641 (2009), [arXiv:0806.4194 \[hep-ph\]](#).
- [22] Adam Alloul, Neil D. Christensen, Celine Degrande, Claude Duhr, and Benjamin Fuks, “FeynRules 2.0 - A complete toolbox for tree-level phenomenology,” (2013), [arXiv:1310.1921 \[hep-ph\]](#).
- [23] Neil D. Christensen, Priscila de Aquino, Celine Degrande, Claude Duhr, Benjamin Fuks, *et al.*, “A Comprehensive approach to new physics simulations,” *Eur.Phys.J. C* **71**, 1541 (2011), [arXiv:0906.2474 \[hep-ph\]](#).
- [24] Celine Degrande, Claude Duhr, Benjamin Fuks, David Grellscheid, Olivier Mattelaer, *et al.*, “UFO - The Universal FeynRules Output,” *Comput.Phys.Commun.* **183**, 1201–1214 (2012), [arXiv:1108.2040 \[hep-ph\]](#).
- [25] Torbjorn Sjostrand, Stephen Mrenna, and Peter Z. Skands, “PYTHIA 6.4 Physics and Manual,” *JHEP* **0605**, 026 (2006), [arXiv:hep-ph/0603175 \[hep-ph\]](#).
- [26] Torbjorn Sjostrand, Stephen Mrenna, and Peter Z. Skands, “A Brief Introduction to PYTHIA 8.1,” *Comput.Phys.Commun.* **178**, 852–867 (2008), [arXiv:0710.3820 \[hep-ph\]](#).
- [27] Michelangelo L. Mangano, Mauro Moretti, Fulvio Piccinini, and Michele Treccani, “Matching matrix elements and shower evolution for top-quark production in hadronic collisions,” *JHEP* **0701**, 013 (2007), [arXiv:hep-ph/0611129 \[hep-ph\]](#).
- [28] N. Davidson, G. Nanava, T. Przedzinski, E. Richter-Was, and Z. Was, “Universal Interface of TAUOLA Technical and Physics Documentation,” *Comput.Phys.Commun.* **183**, 821–843 (2012), [arXiv:1002.0543 \[hep-ph\]](#).
- [29] S. Ovin, X. Rouby, and V. Lemaître, “DELPHEES, a framework for fast simulation of a generic collider experiment,” (2009), [arXiv:0903.2225 \[hep-ph\]](#).
- [30] Jean-Laurent Agram, Jeremy Andrea, Eric Conte, Benjamin Fuks, Denis Gel, *et al.*, “Probing top anomalous couplings at the LHC with trilepton signatures in the single top mode,” *Phys. Lett. B* **725**, 123–126 (2013), [arXiv:1304.5551 \[hep-ph\]](#).
- [31] Matteo Cacciari, Gavin P. Salam, and Gregory Soyez, “FastJet User Manual,” *Eur.Phys.J. C* **72**, 1896 (2012), [arXiv:1111.6097 \[hep-ph\]](#).
- [32] Matteo Cacciari, Gavin P. Salam, and Gregory Soyez, “The Anti-k(t) jet clustering algorithm,” *JHEP* **0804**, 063 (2008), [arXiv:0802.1189 \[hep-ph\]](#).
- [33] Eric Conte, Benjamin Fuks, and Guillaume Serret, “MadAnalysis 5, A User-Friendly Framework for Collider Phenomenology,” *Comput.Phys.Commun.* **184**, 222–256 (2013), [arXiv:1206.1599 \[hep-ph\]](#).
- [34] Eric Conte and Benjamin Fuks, “MadAnalysis 5: status and new developments,” (2013), [arXiv:1309.7831 \[hep-ph\]](#).
- [35] Hung-Liang Lai, Marco Guzzi, Joey Huston, Zhao Li, Pavel M. Nadolsky, *et al.*, “New parton distributions for collider physics,” *Phys.Rev. D* **82**, 074024 (2010), [arXiv:1007.2241 \[hep-ph\]](#).
- [36] Ryan Gavin, Ye Li, Frank Petriello, and Seth Quackenbush, “W Physics at the LHC with FEWZ 2.1,” *Comput.Phys.Commun.* **184**, 208–214 (2013), [arXiv:1201.5896 \[hep-ph\]](#).
- [37] Ryan Gavin, Ye Li, Frank Petriello, and Seth Quackenbush, “FEWZ 2.0: A code for hadronic Z production at next-to-next-to-leading order,” *Comput.Phys.Commun.* **182**, 2388–2403 (2011), [arXiv:1011.3540 \[hep-ph\]](#).
- [38] M. Aliev, H. Lacker, U. Langenfeld, S. Moch, P. Uwer, *et al.*, “HATHOR: HAdronic Top and Heavy quarks crOSS section calculator,” *Comput.Phys.Commun.* **182**, 1034–1046 (2011), [arXiv:1007.1327 \[hep-ph\]](#).
- [39] Nikolaos Kidonakis, “Differential and total cross sections for top pair and single top production,” *JHEP* **1205**, 083 (2012), [arXiv:1205.3453 \[hep-ph\]](#).
- [40] John M. Campbell and R. Keith Ellis, “An Update on vector boson pair production at hadron colliders,” *Phys.Rev. D* **60**, 113006 (1999), [arXiv:hep-ph/9905386 \[hep-ph\]](#).
- [41] John M. Campbell, R. Keith Ellis, and Ciaran Williams, “Vector boson pair production at the LHC,” *JHEP* **1107**, 018 (2011), [arXiv:1105.0020 \[hep-ph\]](#).
- [42] John M. Campbell and R. Keith Ellis, “ $t\bar{t}W^{+-}$ production and decay at NLO,” *JHEP* **1207**, 052 (2012), [arXiv:1204.5678 \[hep-ph\]](#).
- [43] Georges Aad *et al.* (ATLAS Collaboration), “Search for squarks and gluinos using final states with jets and missing transverse momentum with the ATLAS detector in $\sqrt{s} = 7$ TeV proton-proton collisions,” *Phys.Lett. B* **701**, 186–203 (2011), [arXiv:1102.5290 \[hep-ex\]](#).
- [44] Serguei Chatrchyan *et al.* (CMS Collaboration), “Search for New Physics with Jets and Missing Transverse Momentum in pp collisions at $\sqrt{s} = 7$ TeV,” *JHEP* **1108**, 155 (2011), [arXiv:1106.4503 \[hep-ex\]](#).
- [45] Georges Aad *et al.* (ATLAS Collaboration), “Measurement of the t -channel single top-quark production cross section in pp collisions at $\sqrt{s} = 7$ TeV with the ATLAS detector,” *Phys.Lett. B* **717**, 330–350 (2012), [arXiv:1205.3130 \[hep-ex\]](#).
- [46] Serguei Chatrchyan *et al.* (CMS Collaboration), “Measurement of the single-top-quark t -channel cross section in pp collisions at $\sqrt{s} = 7$ TeV,” *JHEP* **1212**, 035 (2012), [arXiv:1209.4533 \[hep-ex\]](#).
- [47] Georges Aad *et al.* (ATLAS Collaboration), “Measurement of WZ production in proton-proton collisions at $\sqrt{s} = 7$ TeV with the ATLAS detector,” *Eur.Phys.J. C* **72**, 2173 (2012), [arXiv:1208.1390 \[hep-ex\]](#).
- [48] Serguei Chatrchyan *et al.* (CMS Collaboration), “Measurement of the sum of WW and WZ production with W +dijet events in pp collisions at $\sqrt{s} = 7$ TeV,” *Eur.Phys.J. C* **73**, 2283 (2013), [arXiv:1210.7544 \[hep-ex\]](#).